

# Gelatin–genipin-based biomaterials for skeletal muscle tissue engineering

Francesca Gattazzo,<sup>1,2</sup> Carmelo De Maria,<sup>2</sup> Alessandro Rimessi,<sup>3</sup> Silvia Donà,<sup>1</sup> Paola Braghetta,<sup>1</sup> Paolo Pinton,<sup>3</sup> Giovanni Vozi,<sup>2</sup> Paolo Bonaldo <sup>1,4</sup>

<sup>1</sup>Department of Molecular Medicine, University of Padova, Padova 35131, Italy

<sup>2</sup>Research Center “E. Piaggio,” University of Pisa, Pisa 56122, Italy

<sup>3</sup>Department of Morphology, Surgery and Experimental Medicine, University of Ferrara, Ferrara 44121, Italy

<sup>4</sup>CRIBI Biotechnology Center, University of Padova, Padova 35131, Italy

Received 7 August 2017; revised 14 November 2017; accepted 18 November 2017

Published online 7 February 2018 in Wiley Online Library (wileyonlinelibrary.com). DOI: 10.1002/jbm.b.34057

**Abstract:** Skeletal muscle engineering aims at tissue reconstruction to replace muscle loss following traumatic injury or in congenital muscle defects. Skeletal muscle can be engineered by using biodegradable and biocompatible scaffolds that favor myogenic cell adhesion and subsequent tissue organization. In this study, we characterized scaffolds made of gelatin cross-linked with genipin, a natural derived cross-linking agent with low cytotoxicity and high biocompatibility, for tissue engineering of skeletal muscle. We generated gelatin–genipin hydrogels with a stiffness of 13 kPa to reproduce the mechanical properties characteristic of skeletal muscle and we show that their surface can be topographically patterned through soft lithography to drive

myogenic cells differentiation and unidirectional orientation. Furthermore, we demonstrate that these biomaterials can be successfully implanted in vivo under dorsal mouse skin, showing good biocompatibility and slow biodegradation rate. Moreover, the grafting of this biomaterial in partially ablated tibialis anterior muscle does not impair muscle regeneration, supporting future applications of gelatin–genipin biomaterials in the field of skeletal muscle tissue repair. © 2018 Wiley Periodicals, Inc. *J Biomed Mater Res Part B: Appl Biomater* 106B: 2763–2777, 2018.

**Key Words:** gelatin, genipin, skeletal muscle, tissue engineering, muscle regeneration

**How to cite this article:** Gattazzo, F, De Maria, C, Rimessi, A, Donà, S, Braghetta, P, Pinton, P, Vozi, G, Bonaldo, P. 2018. Gelatin–genipin-based biomaterials for skeletal muscle tissue engineering. *J Biomed Mater Res Part B* 2018;106B:2763–2777.

## INTRODUCTION

Skeletal muscle is a highly complex organ, mainly characterized by bundles of aligned multinucleated myofibers, necessary for the generation of contraction and strength. One distinct feature of this tissue is its innate capability to regenerate after damage in a highly orchestrated manner, a feature that is largely provided by a specific population of stem cells, named satellite cells.<sup>1</sup> This regenerative capability is impaired under a number of pathological conditions, such as traumatic injury or inherited muscle diseases, and in aging-related sarcopenia.

Muscle tissue engineering approaches aim at repairing or regenerating skeletal muscle by making use of myogenic cells, scaffolds, bioactive molecules, or combination thereof. Toward this aim, in vitro tissue engineering approaches

make use of cells and biomaterials for developing a mature and contractile-engineered muscle construct. In vivo strategies rely upon the transplantation of myogenic cells in skeletal muscle, either alone or in combination with scaffolds that recreate the local microenvironment and allow the integration of cells in the host tissue or promote novel tissue formation. In situ engineering approaches use biomaterials to release multiple bioactive and chemotactic signals and display surface cues to activate, recruit, and reorganize host cell populations, including innervation and vascularization.<sup>2</sup> Although these three strategies display different benefits and limitations, no gold standard methods are currently available for favoring the regeneration of damaged skeletal muscle. Effective in vitro approaches include the culture of myoblasts inside a fibrin gel anchored between two

Additional Supporting Information may be found in the online version of this article.

**Correspondence to:** P. Bonaldo; e-mail: bonaldo@bio.unipd.it

Contract grant sponsor: Italian Association for Cancer Research (AIRC); contract grant number: IG-14442

Contract grant sponsor: Italian Cystic Fibrosis Foundation; contract grant numbers: FFC # 20/2015; FFC #19/2014

Contract grant sponsor: Italian Ministry of Education, University and Research; contract grant numbers: 20129JLHSY\_002; RBAP11FXBC\_002; RBFR10EGVP\_001

Contract grant sponsor: Italian Ministry of Health; contract grant number: GR-2011–02346964

Contract grant sponsor: Italian Ministry of University and Research (FIRB Accordo di Programma); contract grant number: RBAP11Z3YA\_003

Contract grant sponsor: Telethon Foundation; contract grant numbers: GGP11139B; GGP10225; GGP14202

microposts acting as artificial tendons to generate aligned myofibers.<sup>3</sup> Moreover, the addition of factors such as laminin and agrin can stimulate the formation of acetylcholine receptor clusters and their subsequent innervation.<sup>4</sup> Three-dimensional muscle-bundle construct can be implanted in vivo and by incorporating satellite cells in their niche they are capable to exhibit self-repair.<sup>5</sup> PEG-fibrinogen hydrogel carrying mesangioblasts can be injected to generate new muscle in ablated ones.<sup>6</sup> Without extensive culture, combination of myoblasts and alginate scaffolds modified with an Arg-Gly-Asp motif show increase survival and outward migration of myoblasts when implanted in vivo.<sup>7</sup> Moreover, the co-delivery of factors such as VEGF and IGF-1 promote myogenesis and angiogenesis.<sup>8</sup> Decellularized extracellular matrix (ECM)<sup>9</sup> and acellular biomaterial supporting the above mentioned factors<sup>10</sup> can favor regeneration by stimulating myogenesis, vascularization, and innervation, whereas acellular biomaterials can also be specifically designed acting as modulators of the inflammatory response.<sup>11</sup>

In each of the above three strategies, high relevance is given to the realization and optimization of the scaffold. Indeed, optimal scaffolds should (i) support myogenic cell growth and differentiation; (ii) behave as a muscle stem cell niche, by mimicking the native environment to which myogenic cells are exposed<sup>12</sup>; (iii) be biocompatible, to reduce the immune response in the host muscle; (iv) be biodegradable, to gradually allow the substitution of the scaffold by the newly formed muscle.<sup>13</sup> Importantly, one key point is the realization of oriented myofibers. So far, several technologies have been applied to control the orientation of cells and mimic the unidirectional alignment of myotubes, including the fabrication of parallel linear microgrooves,<sup>14–16</sup> the micro-patterning of the surface with tracks of ECM molecules,<sup>17–19</sup> the application of an uniaxial strain in deformable membranes on which cells are grown,<sup>20</sup> the application of electrical excitation,<sup>21</sup> or the use of bioreactors.<sup>22</sup>

Here we propose the use of hydrogels composed of gelatin cross-linked with genipin (GP) for tissue engineering of skeletal muscle. Gelatin, which is essentially denatured collagen, has a myriad of uses in the food, pharmaceutical, and cosmetic industries thanks to its biocompatibility, but shows poor mechanical properties and thermal instability. GP is a naturally occurring and low-cytotoxic crosslinking agent, which is derived from its parent compound geniposide isolated from the fruits of *Gardenia jasminoides Ellis*. GP is able to form stable products with resistance against enzymatic degradation, and is known for its anti-inflammatory and fibrolytic properties.<sup>23–25</sup> GP has been used in the preparation of cross-linked gelatin films and hydrogels,<sup>26,27</sup> for drug delivery purposes,<sup>28,29</sup> and for regenerative applications, including wound dressings,<sup>30</sup> chondrogenic differentiation,<sup>31</sup> nerve guiding conduits,<sup>32,33</sup> cartilage scaffolds,<sup>34</sup> bone scaffolds,<sup>35,36</sup> and arteriogenesis.<sup>37</sup> To our knowledge, gelatin-GP biomaterials were not yet tested for myogenic cell culture or for skeletal muscle applications.

Our results show for the first time that gelatin-GP biomaterials with mechanical properties resembling those of skeletal muscle can support myogenic cell growth,

ameliorate myogenic proliferation, and differentiation, and also guide unidirectional orientation of myotubes when their topology is properly micropatterned. Moreover, our results demonstrate that this material display good biocompatibility and slow biodegradation rate after in vivo implantation. Grafting of acellular gelatin-GP scaffold in injured tibialis anterior (TA) muscle confirmed that the material is not detrimental for muscle regeneration. By displaying all these characteristics, and with the possibility to further modify them in terms of presentation or local delivery of growth factors, we point at gelatin-GP scaffolds as useful biomaterials for skeletal muscle tissue engineering.

## MATERIALS AND METHODS

### Fabrication and characterization of scaffold

Genipin (GP) (Challenge Bioproducts Co., Ltd) was added at 0.2% (w/v) to a solution of gelatin (Sigma) in PBS at different concentrations ranging from 1% to 10% (w/v). Each mixture was kept at 37°C under moderate stirring until polymerization was started, as indicated by turning into blue color. The polymer solution was cast in the mold and the obtained samples were left at room temperature for 48 h until polymerization was complete. The mechanical properties were measured by compressive load-unload cycles using a Zwick/Roell Z005 device with the following settings parameters: 0.01 mm/s, strain rate; 10% strain, end of loading phase; no load, end of load-unload cycle. The Young's modulus of each sample was evaluated from the slope of the initial linear portion of the stress-strain curve. At least 10 specimens for condition were tested.

### Replica molding

A mask with parallel strips of 50, 100, and 200  $\mu\text{m}$  width and 100  $\mu\text{m}$  strip separation was generated. Photoresist (NANOTM SU-8, Microchem) was spun coated onto 10 mm  $\times$  10 mm wafers, producing a 40- $\mu\text{m}$ -thick layer, and the pattern was transferred to the silicon wafer (University Wafers) by exposing to UV light the photoresist through the mask. Then the wafer was developed using MF-319 developer (Microchem) and postbaked at 115°C for 90 s. PDMS solution was prepared (Sylgard 184, Dow Corning), cast onto the topographically patterned photoresist, and cured overnight at 70°C to allow PDMS stamp polymerization. After the fabrication process, the PDMS membrane was removed from the wafer, coated with 0.2% (w/v) pluronic (Invitrogen) to prevent hydrogel adhesion, and covered with 12 ml of gelatin-GP solution. Hydrogel was dried at room temperature and gently detached from the PDMS mold, thus obtaining parallel strips with 50, 100, and 200  $\mu\text{m}$  width, 100  $\mu\text{m}$  strip separation, and 40  $\mu\text{m}$  thickness, and finally cut into pieces (3 mm  $\times$  3 mm), rehydrated in PBS and sterilized for cell seeding. For SEM analysis scaffolds were dried, dehydrated in graded alcohol solution, critical point dried, sputter-coated with gold, and analyzed in a Philips XL 20 scanning electron microscope. For cell seeding, samples were rinsed in PBS to remove GP residues, kept in 70% ethanol overnight, washed with PBS, sterilized under UV light, and kept in PBS until use. Metallic rings were used to

anchor the biomaterial to the well plate during the seeding and culture procedure.

### Cell culture

C2C12 cell line (CRL-1722, ATCC) was cultured and differentiated at 37°C and 5% CO<sub>2</sub>. Cells were expanded in growth medium (DMEM supplemented with 10% fetal bovine serum, 200 mM L-glutamine and 1% penicillin–streptomycin) in T-75 flasks and split 1:3 when cultures reached 80% confluence. Glass cover slips were coated with gelatin 0.1% in PBS and used as control for each experiment. For proliferation analysis, cells were seeded as a single cell suspension at a density of  $10 \times 10^4$  cells cm<sup>-2</sup> onto 13 kPa flat gelatin–GP substrate or glass control and kept in culture for 24 h. For differentiation studies, cells were seeded as a single cell suspension at a density of  $35 \times 10^4$  cells cm<sup>-2</sup> on the flat gelatin–GP substrate and glass control and as droplet on micropatterned gelatin–GP substrates, and cultured for 1 day in growth medium. Cells were then cultured in differentiation medium (DMEM supplemented with 2% horse serum, 200 mM L-glutamine and 1% penicillin–streptomycin) for 7 days to induce myotube formation. Medium was changed and freshly added every 2 days. For primary myoblast cultures, single muscle fibers were isolated from extensor digitorum longus (EDL) of 2-month-old wild-type mice. Freshly isolated satellite cells were stripped off the fibers by repeated passage through an 18-G needle<sup>38</sup>. Debris were then seeded onto a matrigel-coated 35-mm-dish in F10 medium supplemented with 20% fetal bovine serum, 25 ng/ml bFGF, and 1% penicillin/streptomycin (all from Invitrogen). When satellite cells left their parental myofibers and started proliferating, they were trypsinized and expanded in matrigel-coated dishes. SC-derived myoblasts were seeded at  $15 \times 10^4$  cells cm<sup>-2</sup> on micropatterned gelatin–GP substrate and cultured in F10 medium supplemented with 20% fetal bovine serum and 1% penicillin/streptomycin. After one day in proliferation medium, cells were cultured in differentiation media for 7 days as described above.

### Immunofluorescence staining on cells and image analysis

Cells were fixed for 5 min with 4% paraformaldehyde, permeabilized for 10 min in the presence of 0.1% Triton X-100 in PBS, and incubated for 30 min with a blocking solution containing 10% goat serum (Sigma) in PBS. Cells were incubated overnight at 4°C with anti-rabbit Ki-67 (Abcam), antirabbit  $\alpha$ -actin (Sigma), or antimouse myosin heavy chain (MyHC; MF20, Developmental Hybridoma Bank). Slides were incubated for one hour with the following secondary antibodies from Jackson ImmunoResearch: antirabbit Cy2 (1:500) or antirabbit Cy3 (1:1000), antimouse Cy2 (1:500) or antimouse 405 (1:200) diluted in 5% goat serum in PBS solution. Nuclei were stained with Hoechst 33258 (Sigma) or propidium iodide. Slides were mounted in 80% glycerol–PBS and analyzed by fluorescence microscope. The analysis of cell proliferation was performed by calculating the number of nuclei positive for Ki67 on the number of total nuclei, based on images taken at 20 $\times$  magnification. For differentiation analysis only MyHC-positive cells with two or more nuclei were

rated as myotubes. The fusion index was calculated as the ratio of the number of nuclei in myotubes to the number of total nuclei, based on images taken at 20 $\times$  magnification. Myotube alignment was calculated as the angle between the long axis of a myotube and mean orientation axis of the structure (defined as 0°). Myotube orientation score was calculated with the plug-in OrientationJ of ImageJ software from 10 $\times$  magnifications. Myotube length and width were measured using built-in functions of ImageJ software from 10 $\times$  magnification. The 3-D rendering of the micropatterned construct was performed using the ImageJ 3-D View plugin.

### Fura-2/AM measurements

The cytosolic free Ca<sup>2+</sup> concentration ([Ca<sup>2+</sup>]<sub>c</sub>) was evaluated using the fluorescent Ca<sup>2+</sup> indicator Fura-2 acetoxyethyl ester (Fura-2/AM; Molecular Probes). Briefly, cells were incubated in medium supplemented with 2.5  $\mu$ M Fura-2/AM for 30 min, washed with Krebs–Ringer buffer to remove the extracellular probe, supplied with preheated Krebs–Ringer buffer (supplemented with 1 mM CaCl<sub>2</sub>), and placed in a thermostated (37°C) incubation chamber on an Olympus Xcellence system (Olympus Corporation). Fluorescence was measured every 100 ms with the excitation wavelength alternating between 340 and 380 nm and the emission fluorescence being recorded at 510 nm. At the end of the experiment, a region free of cells was selected, and one averaged background frame was collected at each excitation wavelength for background correction. The [Ca<sup>2+</sup>]<sub>c</sub> was calculated by the ratio method using the equation: [Ca<sup>2+</sup>]<sub>c</sub> = Kd (R – R<sub>min</sub>)/(R – R<sub>max</sub>)  $\times$  Sf2/Sf1 where Kd is the dissociation constant of Fura-2/AM for (Ca<sup>2+</sup>) taken as 240 nM at 37°C, R is the ratio of fluorescence for Fura-2/AM at the two excitation wavelengths, F340/F380, R<sub>max</sub> is the ratio of fluorescence in the presence of excess of calcium obtained by lysing the cells with 10  $\mu$ M ionomycin (Sigma Aldrich), R<sub>min</sub> is the ratio of fluorescence in the presence of minimal calcium obtained by lysing the cells and then chelating all the Ca<sup>2+</sup> with 0.5 M EGTA, Sf2 is fluorescence of Ca<sup>2+</sup>-free form of Fura-2/AM at 380 nm excitation wavelength and Sf1 is fluorescence of Ca<sup>2+</sup> bound form of Fura-2/AM at 380 nm excitation wavelength.

### Mice

In vivo experiments were performed in wild-type mice of the inbred C57BL/6NcrJ strain. Mice were housed in individual cages in an environmentally controlled room (23°C, 12 h light/12 h dark cycle) and provided food and water ad libitum. Mouse procedures were approved by the Ethics Committee of the University of Padova and authorized by the Italian Ministry of Health.

### Biocompatibility of biomimetic structures

Four-month-old female C57BL/6NcrJ animals were anesthetized with Avertin (Sigma-Aldrich), the back of the animals was shaved and the exposed skin was treated with povidone-iodine solution to create an aseptic environment at the surgical site. An incision of 1 cm in length was performed and sterile micropatterned biomaterials (3 mm  $\times$  4 mm) were gently implanted subcutaneously in the back.

After implantation, skin was closed using 6/0 Prolene sutures (Ethicon Inc.). Implants were removed upon sacrifice at 1, 3, and 6 weeks after implantation.

### **Surgical implantation of scaffold in injured muscle**

Four-month-old female C57BL/6Ncr1 mice were anesthetized using Avertin (Sigma-Aldrich), and  $\approx 4$  mg wedge of tissue was removed by longitudinal cutting from the core of TA muscles.<sup>39</sup> The removed tissue was weighted to assess the repeatability of the ablation. A micropatterned structure was laid down on the ablation site, and skin was closed using 6/0 Prolene sutures (Ethicon Inc.). The controlateral forelimb received only tissue removal and surgical closure and was used as control.

### **Histological analysis**

Isolated implants with surrounding tissue and TA muscles were frozen in cold isopentane in liquid nitrogen and kept at  $-80^{\circ}\text{C}$  until use. Cross-sections (10  $\mu\text{m}$  thick) were processed with hematoxylin–eosin for body reaction evaluation or Azan–Mallory to identify fibrosis and to quantify capsule thicknesses around implants. Myofiber cross-sectional area was evaluated with the IM1000 software (Leica).

### **Immunofluorescence staining on tissue sections**

Frozen TA sections (8  $\mu\text{m}$  thick) were fixed and permeabilized for 10 min with methanol–acetone at  $-20^{\circ}\text{C}$ , washed in PBS, incubated for 30 min with a blocking solution containing 10% goat serum (Sigma) in PBS. The following primary antibodies were used: rat anti-CD68 (1:300, AbD Serotec); rat anti-CD45 (1:300, Bethyl); rat anti-ER-TR7 (1:300, Santa Cruz); rabbit antilaminin (1:800; L9393, Sigma), rabbit anticollagen IV (1:500, Millipore). After washing, samples were incubated for 1 h at room temperature with the appropriate secondary antibody provided by Jackson ImmunoResearch where not indicated. Secondary biotinylated antimouse antibody (1:1000) was revealed with Cy3 streptavidin (1:1500). Other secondary antibodies used were antirabbit IRIS5 (1:250, Cyanine Technologies); antirabbit CY2 (1:500); antirat Cy3 (1:300). Staining with antibody against mouse Pax7 (1:20; Developmental Studies Hybridoma Bank) was carried out as described<sup>40</sup>. Nuclei were stained with Hoechst 33258 (Sigma). Slides were mounted in 80% glycerol–PBS and analyzed by fluorescence microscopy.

### **Statistical analysis**

Statistical significance for two groups of data was determined by unequal variance Student's *t* test for normally distributed data, or by Mann–Whitney–Wilcoxon test in R for data that were not normally distributed. Statistical significance for multiple comparison data was analyzed using the Kruskal–Wallis one-way ANOVA test followed by Tukey's test using the Matlab Statistic Toolbox (The MathWorks). Data are expressed as mean  $\pm$  standard deviation (s.d.) for the mechanical characterization, and as mean  $\pm$  standard error of the mean (s.e.m) in all the other conditions. A *p* value of  $<0.05$  was considered statistically significant.

## **RESULTS**

### **Gelatin–GP biomaterials sustain cell growth and myogenic differentiation**

By making use of different concentration of gelatin dissolved in PBS (from 2% to 10% weight on total volume) together with a fixed nontoxic concentration of GP (0.2% of total final volume),<sup>35,41</sup> we generated scaffolds with compressive Young modulus ranging from 2 to 75 kPa (Figure 1a). We selected the biomaterial corresponding to a concentration of 4% gelatin (Figure 1a), to mimic the stiffness value in the physiological range of skeletal muscle ( $\approx 12$  kPa), as demonstrated by prior literature studies.<sup>42,43</sup> To test whether the selected biomaterial could allow myogenic differentiation, we seeded C2C12 myogenic cells at subconfluence and we differentiated the cells for 3 days and 7 days, using glass coverslips as a control. Immunofluorescence analysis for the late myogenic differentiation marker MyHC (Figure 1b) and quantification of MyHC-positive myotubes (with  $>2$  nuclei) revealed a significant increase in the number of myotubes grown on the biomaterial compared to glass control at both 3 and 7 days (Figure 1c). The increased number of myotubes on the biomaterial was associated to a higher number of total nuclei compared to glass control (Figure 1d). On the other hand, the fusion index, calculated as the number of nuclei incorporated in myotubes versus the total number of nuclei, was similar for the two conditions (Figure 1e). Myotubes appeared more elongated and narrow when grown on the biomaterial compared to glass control (Figure 1b,f). We found that the increase of total nuclei observed on the biomaterial compared to glass control was linked to a twofold increase in the percentage of proliferating Ki67-positive cells, measured one day after seeding (Figure 1g–i). These data indicate that gelatin–GP biomaterial with 13 kPa favors C2C12 proliferation and myogenic differentiation.

### **Micropatterned gelatin–GP structures promote the orientation and elongation of C2C12 myotubes**

To mimic the organization of skeletal muscle into arranged and aligned myotubes, and based on the fact that the diameter of adult muscle fiber ranges from 10 to 100  $\mu\text{m}$ ,<sup>44</sup> we modified the whole surface of the 13 kPa gelatin–GP material by generating repetitive parallel strips of 50, 100, or 200  $\mu\text{m}$  width, 40  $\mu\text{m}$  height, separated by a deeper 100- $\mu\text{m}$ -wide groove (Figure 2a). When seeded on the micropatterned structures C2C12 cells adhered both to the groove and the strip spacing, and appeared to be oriented in the micropatterning direction since the first day in culture (data not shown). After 7 days of culture in differentiation medium, about 75% of myotubes were unidirectionally aligned on micropatterned structure, at difference from cultures maintained on a nonpatterned flat substrate with the same stiffness (Figure 2b–d). The micropatterned topology was effective in increasing both the elongation (Figure 2e) and the maturity of myotubes, as indicated by the increased nuclear index (i.e., the mean number of nuclei per myotubes)<sup>45</sup> (Figure 2f) and the higher fusion index (Figure 2g). Differentiated C2C12 myotubes did not spontaneously

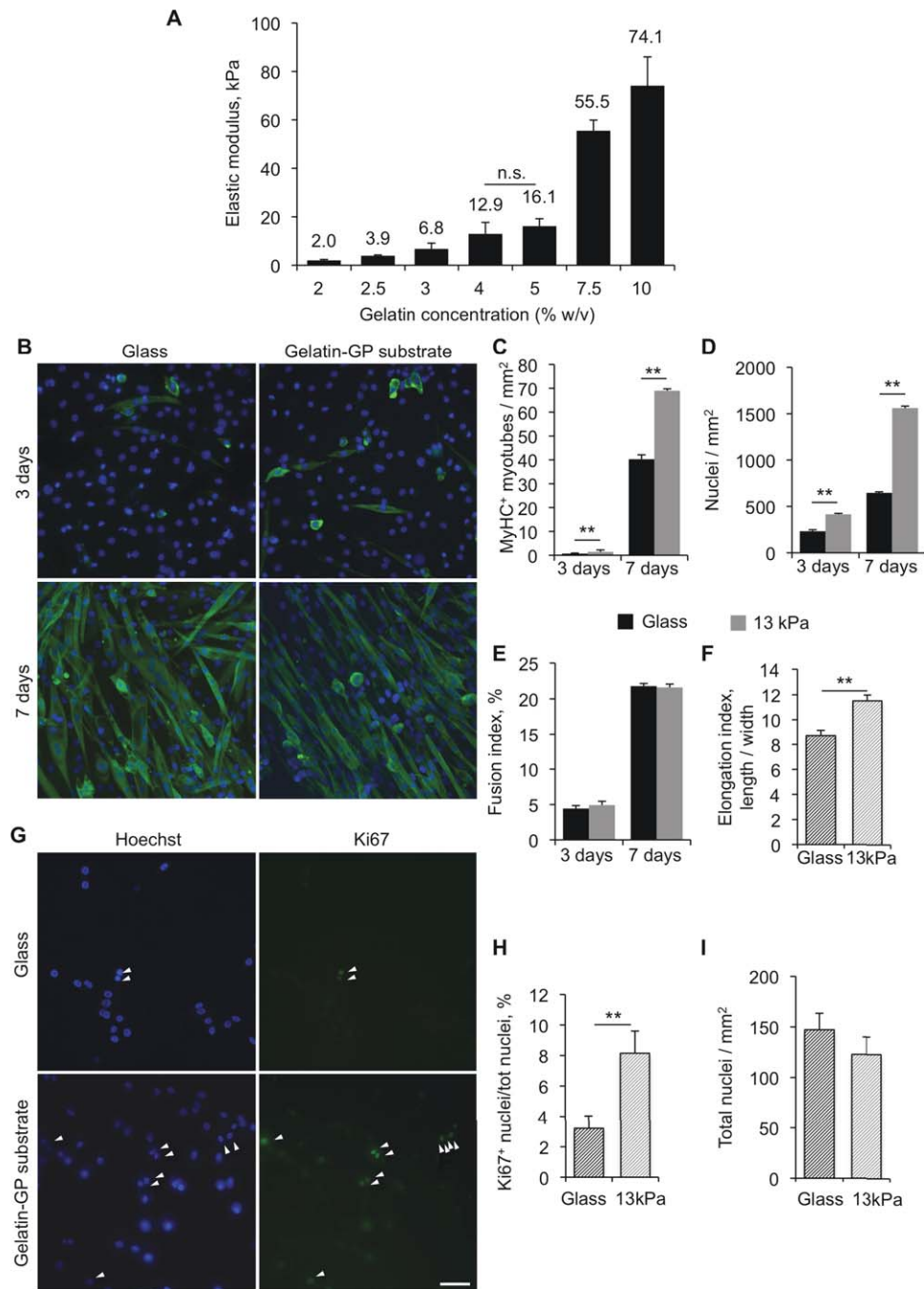


**FIGURE 1.** Gelatin-GP substrates sustain myoblast growth and differentiation. (a) Quantification of the compressive elastic modulus of biomimetic structures composed of gelatin cross-linked with 0.2% GP, as function of increasing concentrations of gelatin (given as % w/v in PBS). Data represent the mean  $\pm$  s.d. of three independent replicates (unequal variance Student's *t* test;  $n = 10$  structures, each group; n.s. not significant.  $P < 0.05$  where not indicated). (b) Immunofluorescence staining for MyHC (green) in C2C12 myotubes differentiated for 3 days or 7 days on glass or on 13 kPa gelatin-GP substrates. Nuclei were stained with Hoechst (blue). Scale bar, 50  $\mu$ m. (c-e) Morphological parameters evaluated on C2C12 myotubes grown for 3 days or 7 days on glass or on 13 kPa gelatin-GP substrates, and corresponding to the quantification of the total number of myotubes per area unit (c), the total number of nuclei per area unit (d), and the fusion index calculated as the percentage of nuclei inside myotubes on total nuclei (e). Error bars indicate s.e.m. (\*\*,  $P < 0.01$ ;  $n = 3$ ). (f) Quantification of elongation index, calculated as the ratio between myotube length and myotube width. Error bars indicate s.e.m. (\*\*,  $p < 0.01$ ;  $n = 3$ ). (g) Immunofluorescence staining for Ki67 (green) on C2C12 cell cultures grown for 24 h on glass or on 13 kPa gelatin-GP substrates. Nuclei were stained with Hoechst (blue). Scale bar: 50  $\mu$ m. (h) Percentage of proliferating C2C12 cells grown on glass or on 13 kPa gelatin-GP substrates, calculated as Ki67-positive nuclei on total nuclei. Error bars indicate s.e.m. (\*\*,  $p < 0.01$ ;  $n = 3$ ). (i) Quantification of the total number of nuclei per area unit of C2C12 cells grown on glass or on 13 kPa gelatin-GP substrates. Data are expressed as mean  $\pm$  s.e.m. (not significant;  $n = 3$ ).

contract in culture, neither on glass nor on the biomaterial, and only few striations were noticed on the micropatterned biomaterial but not on glass control (Supporting

Information, Figure S1). To assess the functionality of myotubes in our culture system, we measured cytosolic free  $\text{Ca}^{2+}$  concentrations by making use of Fura-2/AM calcium-

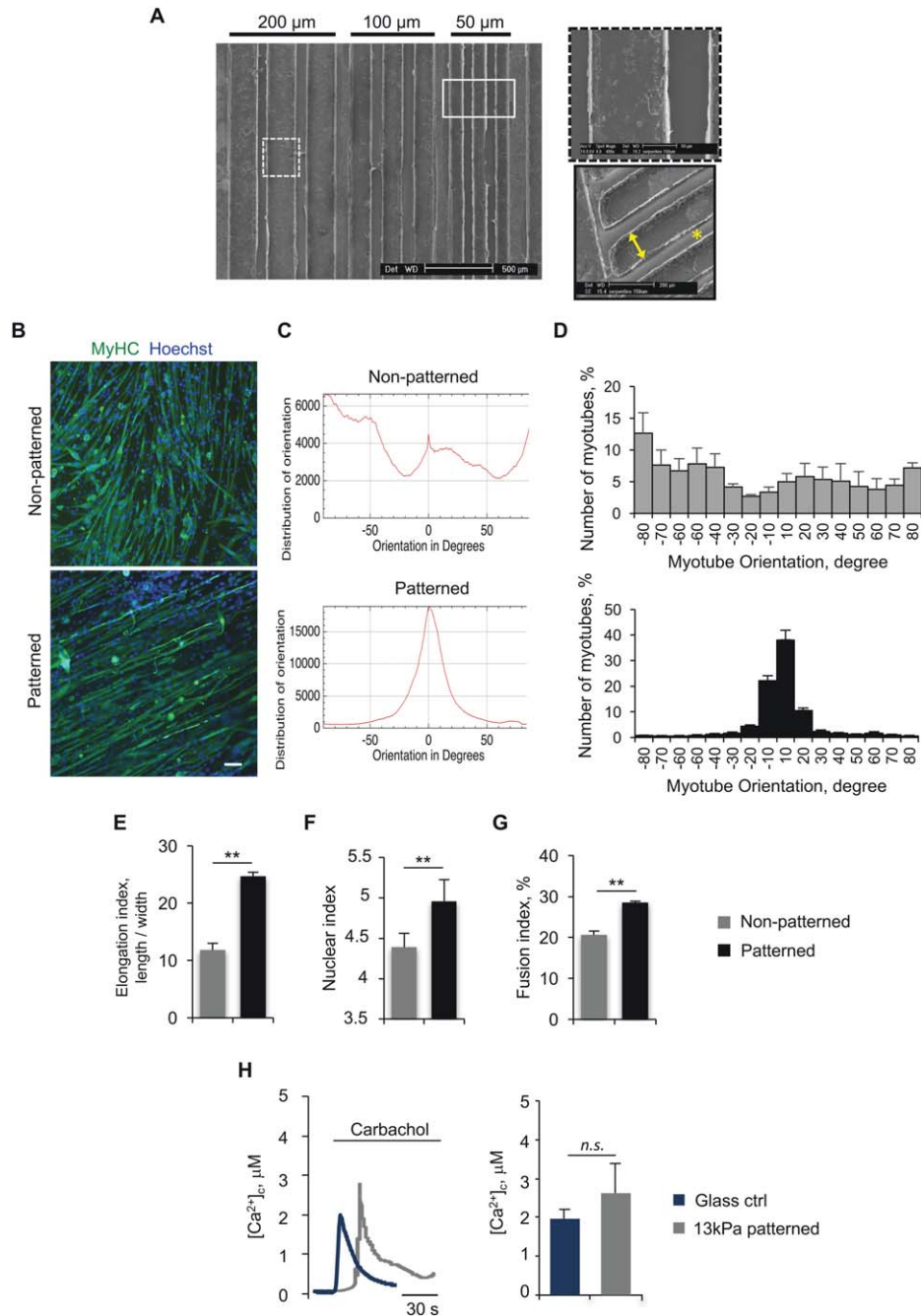


**FIGURE 2.** Micropatterned gelatin–GP substrates promote the alignment, elongation, and fusion of myoblasts. (a) Scanning electron microscope analysis of dry graded aligned structures. The aligned strips are 200, 100, and 50 μm wide, 40 μm high, and 100 μm apart. Higher magnifications of frontal view (upper panel) and lateral view (lower panel) are shown on the right. Arrowed line indicates the width of channel separation, asterisk highlights the 40 μm high channel. (b) Immunofluorescence staining for MyHC (green) in C2C12 myotubes differentiated for 7 days on nonpatterned or micropatterned gelatin–GP substrates with a stiffness of 13 kPa. Nuclei were stained with Hoechst (blue). Scale bar: 75 μm. (c–f) Quantification of morphological parameters of C2C12 myotubes differentiated for 7 days on nonpatterned and micropatterned gelatin–GP substrates, and corresponding to: representative plot of the distribution of myotubes orientation obtained by OrientationJ software analysis (c); distribution of myotube orientation, calculated in respect to the main direction of the micro-patterning (d); elongation index, calculated as the ratio between myotube length and myotube width (e); nuclear index, calculated as the mean number of nuclei inside myotubes (f); fusion index, calculated as the percentage of nuclei inside myotubes on total nuclei (g). Data are expressed as mean ± s.e.m. (\*\*,  $p < 0.01$ ;  $n = 5$ ). (h) Analysis of calcium fluxes with Fura-2/AM after carbachol stimulation of C2C12 myotubes differentiated for 7 days on micropatterned 13 kPa gelatin–GP substrates and on glass coverslips control. The left panel shows the cytosolic calcium concentrations ( $[Ca^{2+}]_i$ ) at different times after carbachol stimulation, whereas the right panel shows the quantification of the peak calcium levels of different myotubes. Error bars indicate s.e.m. ( $n = 5$ ). n.s., not significant.

sensitive dye (Figure 2h). Generation of  $Ca^{2+}$  fluxes demonstrated that myotubes grown on the micropatterned biomaterial were responsive to carbachol administration, thus

providing a proof of concept of the feasibility of the use of micropatterned gelatin–GP biomaterials for electrophysiological studies. Despite a slight increasing in the trend, no

significant difference in the value of cytosolic free  $\text{Ca}^{2+}$  concentrations was observed in comparison with glass control (Figure 2h). Altogether, these data indicate that micropatterned gelatin-GP biomaterials are effective in guiding myotube orientation and promoting myotube differentiation.

### Strip spacing influences the alignment of C2C12 myotubes

We then evaluated the contribution of strip spacing on the alignment of myotubes. Matrix topography was found to elicit a substantial effect on myotube size and orientation (Figure 3). Not only myotubes were aligned in the groove spacing, but they were also aligned on upper strips (Figure 3a,b and Supporting Information, Figure S2). The mean orientation degree was under  $10^\circ$  for each microconstruct width considered, and the best orientation was observed on 50 and 100- $\mu\text{m}$ -wide spacing. Interestingly, the topology dimension appeared to be the driving force of alignment, since no significant difference was observed between 100- $\mu\text{m}$ -wide groove and 100- $\mu\text{m}$ -wide spacing. No significant difference was found between 50- and 100- $\mu\text{m}$ -wide strips, indicating that 100  $\mu\text{m}$  may be the optimal size for a material with a fixed groove and strip spacing (Figure 3c). On the wider strips with 200  $\mu\text{m}$  width, myotubes were significantly less oriented when compared to the narrower strips and groove spacing, and myotubes appeared significantly shorter and larger when compared to 50- and 100- $\mu\text{m}$ -wide strips (Figure 3e,f), despite a similar nuclear index (Figure 3d). No significant differences were observed in the length and width of myotubes cultured on 50- and 100- $\mu\text{m}$ -wide strips (Figure 3e,f).

### Micropatterned gelatin-GP structures promote the orientation of primary myotubes

To test the feasibility of the chosen gelatin-GP biomaterial in sustaining the culture of primary myoblasts, we isolated satellite cells from mouse EDL muscle and differentiated them into myoblasts that were then cultured on the micropatterned structures. Primary myoblasts attached to gelatin-GP substrates without any coating, with a preference on the strip spacing compared to the groove spacing, and were able to differentiate on the substrates, as shown by immunofluorescence staining for MyHC at 7 days culture in differentiation medium (Figure 4a). At this time point, myotubes were aligned on each groove spacing, as shown by an orientation degree lower than  $10^\circ$ , but myotubes grown on 50  $\mu\text{m}$  showed a better orientation when compared to 200- $\mu\text{m}$ -wide strips (Figure 4b). Primary myotubes were less sensitive than C2C12 myotubes to the topology of the biomaterial, as no significant difference was observed in their nuclear index, and in myotube length and width, among 50-, 100-, and 200- $\mu\text{m}$ -wide strips (Figure 4c–e). Notably, and at difference from C2C12-derived myotubes, primary myotubes were capable to spontaneously contract on the biomaterial and higher magnification revealed the formation of sarcomeric structures (Figure 4f and Supporting Information, Movie).

### Gelatin-GP scaffolds are biocompatible in vivo and display a slow biodegradation rate

We then investigated the feasibility to use such materials not only for in vitro but also for in vivo applications. Toward this aim, we performed an incision (1 cm in length) in the dorsal skin of wild-type mice and implanted subcutaneously a micropatterned structure (0.3 cm  $\times$  0.5 cm). The biocompatibility of the material was evaluated at 1, 3, and 6 weeks after implantation. Macroscopic examination revealed the absence of any sign of edema or rash soon after the surgery and at different time points after implantation, indicating that the material did not elicit rejection responses. Interestingly, given its deep blue color, the structure could be easily identified under the skin (Supporting Information, Figure S3). Hematoxylin-eosin staining confirmed that the structure was still present after 6 weeks from implantation, but its thickness appeared reduced and its internal porosity increased (Figure 5a). In addition, the surface appeared more irregular and undergoing a degradation process (Figure 5a), as indicated by a layer of mononucleated cells that persisted around the structure for all the time points considered. Interestingly, at 7 days from implantation, some mononucleated cells were adherent on the biomaterial surface both on the upper and lower sides, whereas they began to appear in the more internal region of the substrate at 3 and 6 weeks from implantation (Figure 5a). Azan-Mallory staining showed a fibrotic capsule surrounding the biomaterial, and morphometric analysis indicated that its thickness reached a peak 3 weeks after implantation but was significantly reduced after 6 weeks (Figure 5b,c). Immunofluorescence staining for the main cell populations involved in the foreign body reaction indicated that the majority of cell recruited in the site of implantation were macrophages (CD68-positive cells) and fibroblasts (ER-TR7-positive cells), with some of those cells adherent onto the structure at 7 days from implantation (Figure 5d). Notably, their number increased at 3 and 6 weeks from implantation, and those cells were found invading the structure and surrounding its degrading parts (Figure 5d). These findings reveal that the inflammatory resolution stage was ongoing, thus showing that micropatterned gelatin-GP structures are biocompatible and biodegradable, and indicating that the degradation time and the reabsorbance of the fibrotic tissue capsule take  $>6$  weeks.

### Gelatin-GP biomaterials do not impair skeletal muscle regeneration

We next evaluated the feasibility of engrafting micropatterned gelatin-GP structures in murine TA muscle. To reproduce a condition in which biomaterial construct implantation is needed, such as muscle damage, we subjected TA muscle to a partial muscle ablation. Ablation of myofibers was chosen in order to stimulate muscle regeneration and at the same time generate an empty space that can be taken over by the biomaterial itself (Supporting Information, Figure S4). Histological analysis revealed that the partial ablation of muscle fibers was efficient in inducing regeneration in a limited portion of the external region

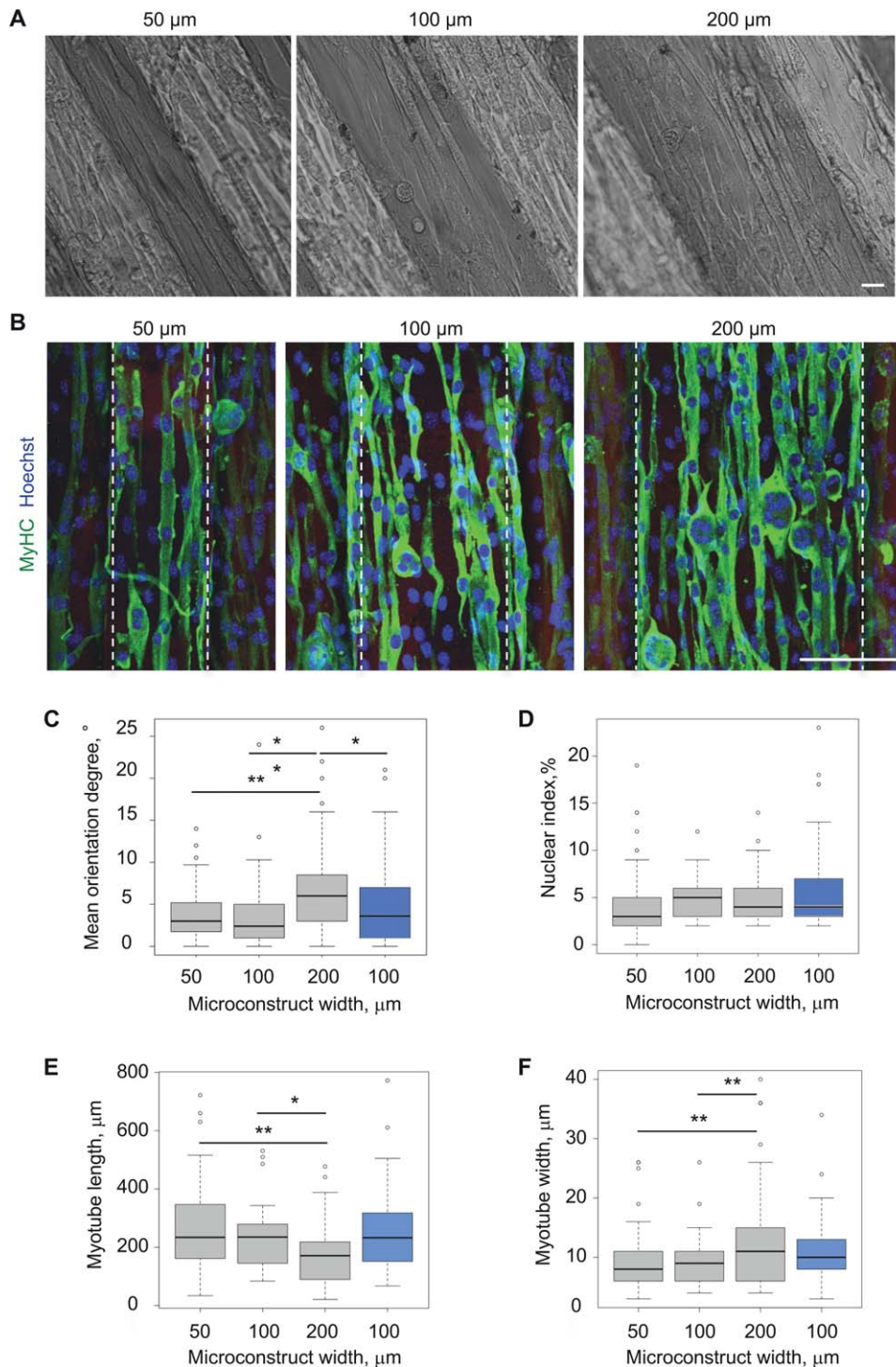


**FIGURE 3.** Strip spacing of micropatterned gelatin–GP structures influences C2C12 myotubes. (a) Representative light microscopy images of C2C12 myoblasts cultured in differentiation medium for 7 days onto 12 kPa gelatin–GP micropatterned structures with 50, 100, or 200  $\mu\text{m}$  wide strips. Scale bar, 75  $\mu\text{m}$ . (b) Immunofluorescence staining for MyHC (green) on C2C12 differentiated for 7 days onto 13 kPa micropatterned GP–gelatin biomaterial with 50, 100, or 200  $\mu\text{m}$  wide strips. Nuclei were stained with Hoechst (blue). Scale bar: 100  $\mu\text{m}$ . (c) Quantification of the orientation degree of C2C12 myotubes grown on 50, 100, or 200  $\mu\text{m}$  wide strips (black) and 100  $\mu\text{m}$  groove (light blue) (\*\*,  $p < 0.01$ ; \*,  $p < 0.05$ ;  $n = 3$ ). (d) Quantification of the nuclear index of C2C12 myotubes cultured on 50, 100, or 200  $\mu\text{m}$  wide strips (black) and 100  $\mu\text{m}$  groove (light blue) (not significant;  $n = 3$ ). (e,f) Quantification of the average length (e) and of the average width (f) of C2C12 myotubes cultured on 50, 100, or 200  $\mu\text{m}$  wide strips (black) and 100  $\mu\text{m}$  groove (light blue) (\*,  $p < 0.05$ ; \*\*,  $p < 0.03$ ;  $n = 3$ ). At least 300 myotubes were considered for each condition.

of TA, and that the cross-sectional area of regenerating centrally nucleated myofibers increased with time, with only a slight significant difference between control and grafted

animals despite the inflammatory process and the presence of mononucleated cells in the latter (Figure 6a,b). To verify the identity of infiltrating cells surrounding and adhering to

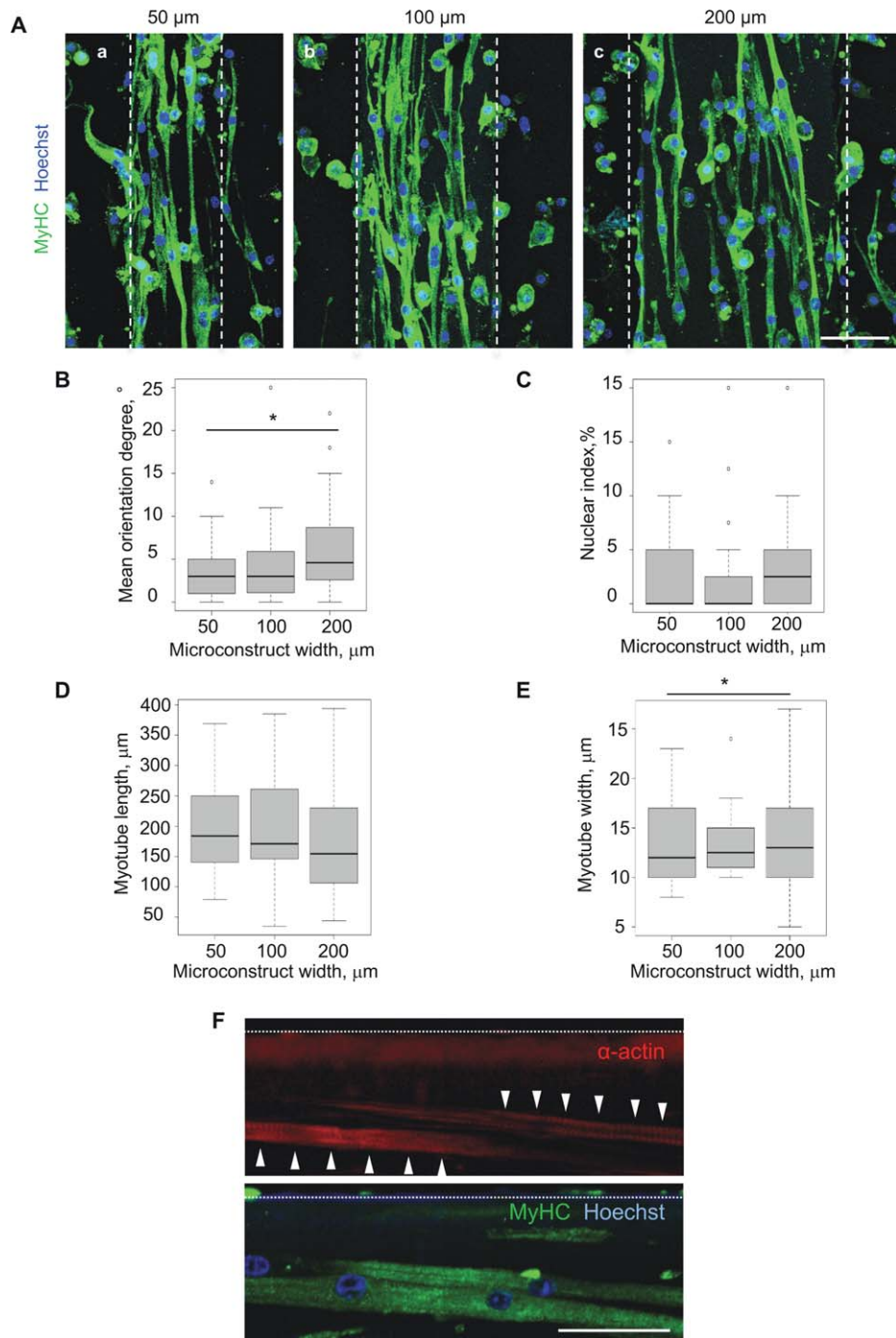


**FIGURE 4.** Micropatterned gelatin-GP biomaterials guide the orientation of primary myotubes. (a) Immunofluorescence staining for MyHC (green) of primary mouse myotubes cultured for 7 days onto 13 kPa micropatterned GP-gelatin structures with 50, 100, or 200  $\mu\text{m}$  wide strips. Nuclei were stained with Hoechst (blue). Scale bar, 75  $\mu\text{m}$ . (b) Quantification of the orientation degree of primary mouse myotubes grown on 50, 100, or 200  $\mu\text{m}$  wide strips (\*,  $p < 0.05$ ;  $n = 3$ ). (c) Quantification of the nuclear index of primary mouse myotubes cultured on 50, 100, or 200  $\mu\text{m}$  wide strips (not significant;  $n = 3$ ). (d,e) Quantification of the average length (d) and of the average width (e) of primary mouse myotubes cultured on 50, 100, or 200  $\mu\text{m}$  wide strips (\*,  $p < 0.05$ ;  $n = 3$ ). At least 100 myotubes were considered for each condition. (f) Immunofluorescence staining for MyHC (green) and  $\alpha$ -actin (red) in primary wild-type myotubes cultured on micropatterned structures. The arrows point at the developing contractile apparatus. The dotted line indicates strip spacing. Scale bar: 25  $\mu\text{m}$ .

the surface of the biomaterial, we performed immunofluorescence for different regenerative and inflammatory markers. At 7 days after muscle damage, no Pax7-positive satellite cell was found adherent on the surface of the

structure or in the more proximal region adjacent to the structure, indicating that the structure alone did not attract satellite cells, which were found associated with myofibers in both control and grafted TA (Figure 6c). As observed in

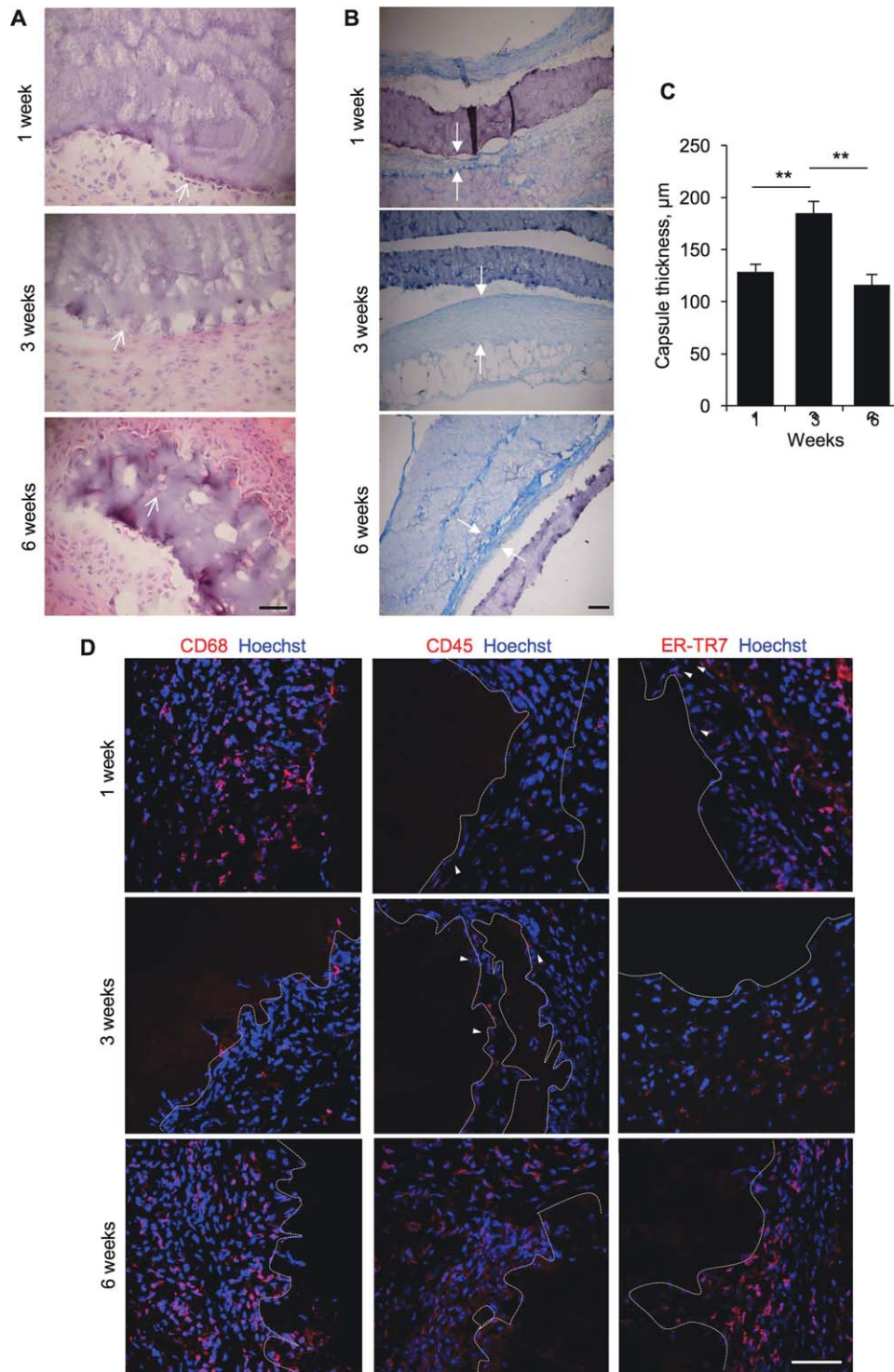


**FIGURE 5.** Analysis of subcutaneous in vivo grafting of micropatterned gelatin-GP scaffolds under mouse dorsal skin. (a) Hematoxylin-eosin staining of mouse back skin sections at 1, 3, and 6 weeks after subcutaneous implantation of micropatterned gelatin-GP biomaterial. The arrows point at some mononucleated cells adherent or infiltrating the implanted structure. Scale bar: 50  $\mu\text{m}$ . (b) Azan-Mallory staining of mouse back skin sections at 1, 3, and 6 weeks after subcutaneous implantation of the micro-patterned biomaterial. The arrows mark the fibrotic tissue capsule surrounding the implant. Scale bar: 100  $\mu\text{m}$ . (c) Quantification of the thickness of the foreign body capsule at 1, 3, and 6 weeks after subcutaneous implantation of the micropatterned biomaterial. Error bars indicate s.e.m. (\*\*,  $p < 0.03$ ;  $n = 3$  animals, each group). (d) Immunofluorescence staining for CD68, CD45, and ER-TR7 (red) of subcutaneous tissue sections at 1, 3, and 6 weeks after subcutaneous implantation of the micropatterned biomaterial. Nuclei were stained with Hoechst (blue). The dotted black areas mark the micropatterned scaffold. The arrowheads point at some cells adherent to the scaffold. Scale bar: 50  $\mu\text{m}$ .

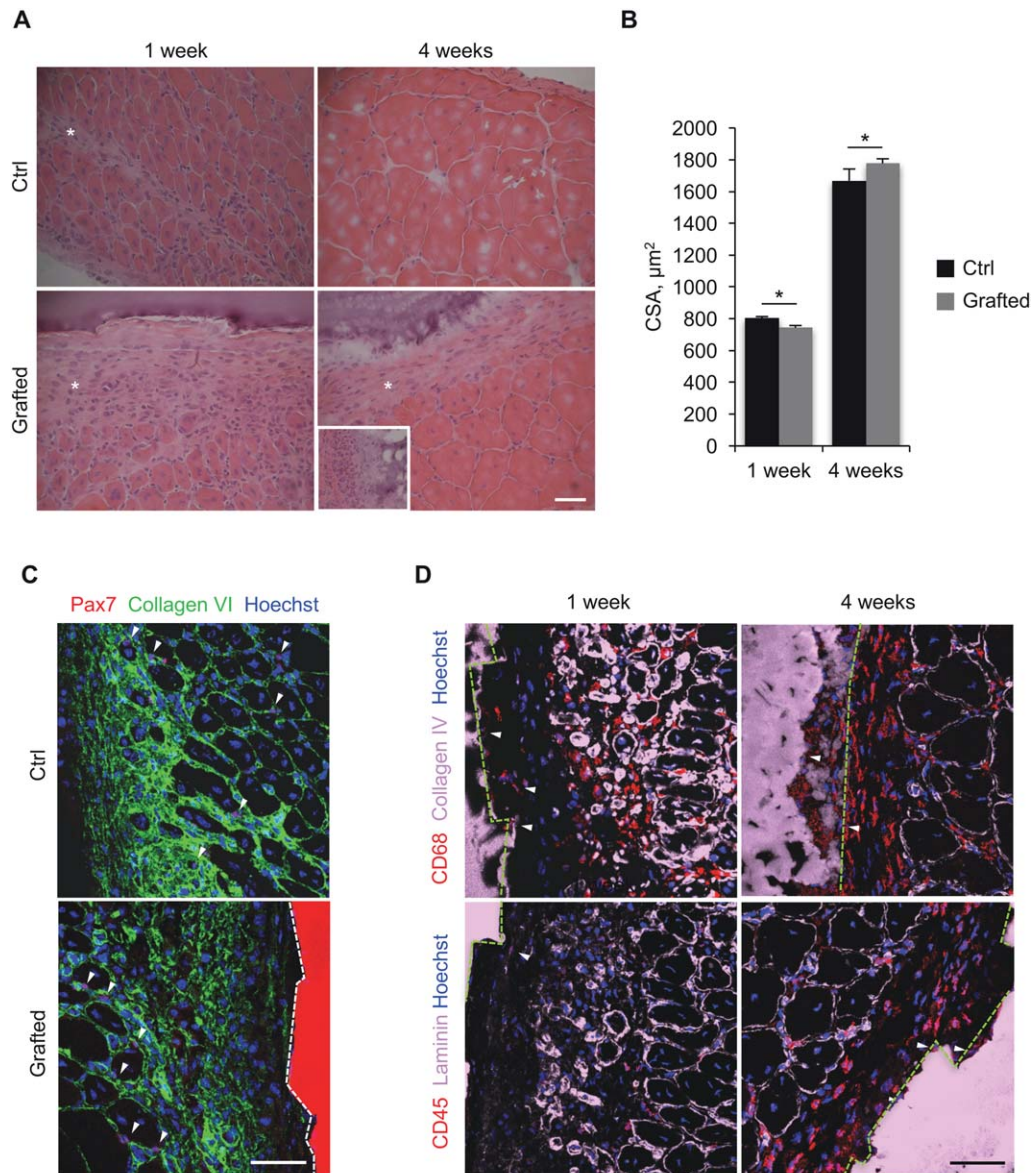


**FIGURE 6.** Analysis of injured mouse TA muscles grafted with micropatterned gelatin–GP scaffolds. (a) Hematoxylin–eosin staining of mouse TA cross-sections 1 and 4 weeks after partial surgical muscle ablation (Ctrl) and grafting with the micro-patterned gelatin–GP biomaterial (Grafted). The asterisks mark some mononucleated cells. The inset shows mononucleated cells invading the biomaterial at the borders. Scale bar, 100  $\mu\text{m}$ . (b) Mean cross-sectional area (CSA) of centrally nucleated fibers 1 and 4 weeks after partial surgical muscle ablation (Ctrl) and grafting with the micro-patterned biomaterial (Grafted). Error bars indicate s.e.m. (\*\*,  $p < 0.03$ ;  $n = 3$  animals, each group). (c) Double immunofluorescence labeling for collagen VI (green) and Pax7 (red) of mouse TA cross-sections 7 days after partial surgical muscle ablation (Ctrl) and after grafting with the micro-patterned biomaterial (Grafted). Nuclei were stained with Hoechst (blue). Arrowheads point at some Pax7-positive cells. The dotted area marks the autofluorescent scaffold. Scale bar: 50  $\mu\text{m}$ . (d) Double immunofluorescence labeling for CD68 (red) and collagen IV (pink, upper panels) or laminin (pink, lower panels) of mouse TA cross-sections 1 and 4 weeks after grafting with the micropatterned biomaterial in the damaged region. Nuclei were stained with Hoechst (blue). Arrowheads point at some adherent cells. The dotted areas mark the autofluorescent scaffold. Scale bar: 50  $\mu\text{m}$ .

the dorsal skin implantation experiments, the majority of cells found in the proximity of the structure, at both 7 days and 1 month after damage, were CD68-positive macrophages and CD45-positive cells (Figure 6d and Supporting Information, Figure S5). CD45- and CD68-positive cells were already attached on the biomaterial surface at 7 days after implantation and their number increased at 1 month, where cells were also infiltrating inside the structure. These

findings indicate that the degradation of the grafted structure was undergoing, but the degradation process is slow and takes  $>4$  weeks.

## DISCUSSION

In this work, we investigated the use of biomaterials composed of gelatin cross-linked with GP for skeletal muscle

tissue engineering applications and we tested their *in vitro* and *in vivo* biocompatibility. Our results show for the first time that besides their use for bone, nerve, and cartilage repair and arteriogenesis,<sup>34,35,37,46</sup> gelatin-GP biomaterials may find application also in the field of skeletal muscle regeneration, thanks to the possibility to modulate their mechanical properties and 3-D architecture, and to their biocompatibility for myogenic cell culture.

One of the advantages of this material relies on its tunable mechanical properties, leading to the generation of a broad range of stiffness values (from 2 to 75 kPa in our study), including those of skeletal muscle. We selected gelatin-GP biomaterials with a stiffness value of 13 kPa, thus mimicking the elastic modulus previously published for skeletal muscle<sup>42,43</sup> and we observed an increase in the proliferation of C2C12 cells and in the number of differentiated myotubes, when compared to glass control. These results demonstrate that this biomaterial is capable not only to sustain and favor the proliferation of myogenic cells, but also to improve the myogenic differentiation, two events that are necessary for the regeneration of a functional skeletal muscle. Moreover, these findings are in agreement with literature data, showing that myogenic differentiation is promoted by stiffness values in the range of 10–15 kPa,<sup>47</sup> and that natural alginate hydrogel with stiffness values between 13 and 45 kPa increases myoblast proliferation and differentiation.<sup>48</sup> Besides the generation of myotubes, the guidance of their anisotropic alignment is an essential condition for mimicking the native skeletal muscle. In agreement with other studies on both rodent and human myogenic cells,<sup>14,45,49–56</sup> we observed that patterning the substrate surface is an efficient method to drive myotube orientation. The amelioration in the elongation and orientation index of myotubes cultured on materials with strips of different width is triggered by a reorganization of the cytoskeleton in response to the cues provided by surface features. Similar to strip width, it is known that grooves with a height >10  $\mu\text{m}$  lead to a physical restriction of cells.<sup>56</sup> Our results show that C2C12 cells and primary myoblasts are nicely unidirectionally oriented when they are cultured on 13 kPa graded gelatin-GP biomaterial with 50-, 100-, and 200- $\mu\text{m}$ -wide strips, separated by fixed 100  $\mu\text{m}$  grooves of 40  $\mu\text{m}$  height. Notably, both C2C12 cells and mouse primary myoblasts exhibit a higher alignment on substrates with smaller groove spacing. We did not characterize in detail the impact of the strip width on some cellular parameters, such as the proliferation rate or the fusion index. Nevertheless, our results are in agreement with previous studies showing the beneficial effect of a similar range of strips sizes (from 50 to 500  $\mu\text{m}$ ) on the alignment and orientation of myogenic cells<sup>17,18,54,57,58</sup> Altogether, our data reveal that the patterning of the biomaterial promoted a higher rate of myotube maturation in terms of fusion index and nuclear index when compared to unpatterned substrates, further increasing the capability of gelatin-GP biomaterial to induce myogenic differentiation. However, at difference from other works, C2C12 showed only a slight appearance of striations both on the biomaterial and on the glass control, a result that

may rely upon the selected batch of cells. Differently, primary myotubes spontaneously contracted when cultured onto micropatterned substrates. Although future studies will be required to enhance and optimize culture conditions, our present results provide a proof of concept of the feasibility of the use of micropatterned gelatin-GP biomaterial to generate *in vitro* cultures of unidirectionally aligned contracting primary myotubes where electrophysiological studies can be performed. A recent study showed that micropatterned gelatin hydrogels, realized with different cross-linker and smaller strip size, are more effective in driving the growth and orientation of C2C12 myotubes in *in vitro* long-term cultures, when compared to the commonly used extracellular microcontact printed PDMS.<sup>59</sup> Although we did not analyze our cells after 3 weeks in culture, we could assume that our system may be as effective as this, and find application for *in vitro* studies on muscle development and disease, and on chronic drug testing.

One of the potential drawbacks of GP is the generation of a blue colored structure that displays strong autofluorescence. Although on one hand this limits the use of immunofluorescence staining,<sup>60</sup> on the other hand, it is extremely useful for the detection of the implanted biomaterial after *in vivo* grafting. To obtain a further characterization of the material for *in vivo* applications, we engrafted micropatterned gelatin-GP structures either under dorsal skin or on injured TA muscle of nonimmunodeficient mice. The choice of implanting the micropatterned biomaterial, instead of the flat one, was due to the interest in assessing the features of a material capable to orient myoblasts, in the perspective to use it in the future with embedded myogenic cells. In our experimental setting, both skin and muscle grafting revealed that the acellular micropatterned gelatin-GP material was well received, showing a biodegradability of over than 6 weeks. It should be considered that in our experimental approach scaffolds were not fixed with glue or suture, therefore will be interest in the next future to investigate the impact of fixation protocols on the regeneration outcome and on the permanence and stability of the implanted scaffold. However, our results are consistent with the long biodegradation rate observed for gelatin-GP cross-linked materials in peripheral nerve guide conduit, either alone or embedded with adipose-derived stem cells.<sup>32,46</sup> Although in those studies the mechanical properties of the material were not characterized, the authors reported that a 0.11- to 0.15-mm-thick conduit was still present after 8 weeks, despite some signs of degradation at 6 weeks and a thin fibrotic capsule around the structure.<sup>46</sup> It can be hypothesized that the long biodegradation rate of the implanted micropatterned gelatin-GP biomaterial may be linked to its thickness ( $\sim 200 \mu\text{m}$ ), suggesting that this aspect may represent a critical parameter for tissue engineering applications. On the one side, for skeletal muscle application it would be desirable that the degradation rate of the implanted material lasts about 4–6 weeks, corresponding to the rate of new tissue formation,<sup>8</sup> implying that the biomaterial thickness should be reduced. Nevertheless, the biodegradation time of several natural biomaterials used for skeletal muscle application are variable, varying

from up to 12 weeks for decellularized muscle ECM<sup>61,62</sup> or limited to 39 days for alginate gels,<sup>63</sup> based on their different composition, cross-linking, dimension, and internal porosity. On the other side, a long biodegradation should be desirable in the case of muscles necessary to support specific anatomical locations, such as the abdominal wall, or for the long-lasting release of drugs.

One of the main issues associated with protein-based scaffolds is immune rejection and the onset of a foreign body response,<sup>64</sup> leading to many *in vivo* studies being carried out in immunodeficient animal models, at a difference from our study. Our analysis revealed the presence of macrophages and inflammatory cells degrading the structure at 3 and 6 weeks after implantation. Furthermore, our data indicate that the long permanence of the biomaterial alone did not interfere with muscle regeneration in our model of TA injury. Further studies will be aimed at evaluating the timing of complete degradation of the material and of the fibrotic capsule, together with a more detailed analysis of the inflammatory response in terms of macrophage polarization. Persistent macrophage polarization into M1 is associated with fibrotic and scar tissue formation, whereas anti-inflammatory M2 macrophages are known to guide the resolution of the inflammatory stage and also to stimulate the proliferation and differentiation of satellite cells toward the formation of new fibers.<sup>65,66</sup> Given the naturally derived origin of our biomaterial, it would be worthy to carefully investigate whether gelatin-GP scaffolds may promote the switch of macrophages from an M1 to an M2 phenotype, as it was observed during the degradation of decellularized skeletal muscle ECM implants.<sup>67</sup> On the other hand, the use of nude mice or mice with immunodeficient background should be taken into account for the purpose of grafting experiments using biomaterials embedded with cells, considering that such experimental approaches may lead to some bias. For example, Ma et al. used a porous collagen scaffold seeded with murine myoblasts for the treatment of skeletal muscle defects, and reported that although vascularization, innervation, and the generation of myofibers were observed, successful integration of the scaffold-tissue graft was only evident in immune-compromised animals.<sup>68</sup>

Differently from acellular decellularized scaffolds, which show the capability to support the infiltration of myogenic cells,<sup>69,70</sup> in our grafting experiments, we observed that the biomaterial alone did not recruit satellite cells on its surface. Thus, future work will be aimed at assessing the impact of gelatin-GP biomaterial embedded with myogenic cells. A literature study suggested the use of predifferentiated myotubes instead of undifferentiated satellite cells, as they elicit an increased invasion of host vessels in avascular muscle bundles after 14 days from implantation in dorsal skin.<sup>5</sup> In our case, the long lasting of the implanted structure in TA muscle and the maintenance of its topology during time suggest the feasibility of the use this material for the grafting of unidirectional aligned myotubes for *in vivo* muscle engineering applications. Yang et al. for example, showed that the transplantation of differentiated primary muscle cells onto a biodegradable gelatin-coated

nanopatterned PLGA substrate allows for the integration in the host musculature and lead to the formation of a significantly higher number of dystrophin-positive muscle fibers, when compared to unpatterned patches, in the *mdx* dystrophic mouse model.<sup>71</sup> The detailed analysis of the combinatory effects of patterned biomaterial and cells in terms of myogenic response, degradation profile, and macrophage recruitment are intriguing aspects that remain to be investigated in the context of our gelatin-GP scaffold. Additionally, and similarly to other natural hydrogels, one advantage of gelatin-GP biomaterial is represented by the feasibility to finely tune its properties,<sup>29</sup> so that future modifications of the micropatterned gelatin-GP biomaterial may include the presentation or local delivery of growth factors such as IGF-1 and VEGF,<sup>8,10,71</sup> or the modulation of the inflammatory response focused to control the polarization of macrophages toward the M2 phenotype.<sup>11,72,73</sup> For example, Wang et al. showed that the injection of a combination of shape memory alginate gel, with embedded myogenic cells and growth factors (IGF-1 and VEGF), did not only increase the regeneration outcome after cardiotoxin damage, but also reduced the fibrotic tissue compared to the injury alone or the injection of cells and factors without scaffold.<sup>8</sup> Therefore, the addition of selected growth factors will be considered for the future implementation of this gelatin-GP biomaterial both for *in vitro* and *in vivo* applications.

Altogether, these results provide the first characterization for the novel use of gelatin-GP biomaterial for *in vitro* and *in vivo* applications in the field of skeletal muscle tissue engineering.

#### ACKNOWLEDGMENT

Paolo Pinton is grateful to Camilla degli Scrovegni for continuous support.

#### AUTHOR DISCLOSURE STATEMENT

The authors declare no potential conflicts of interest. No competing financial interests exist.

#### REFERENCES

1. Zammit PS, Relaix F, Nagata Y, Ruiz AP, Collins CA, Partridge TA, Beauchamp JR. Pax7 and myogenic progression in skeletal muscle satellite cells. *J Cell Sci* 2006;119:1824–1832.
2. Qazi TH, Mooney DJ, Pumberger M, Geißler S, Duda GN. Biomaterials based strategies for skeletal muscle tissue engineering: Existing technologies and future trends. *Biomaterials* 2015;53:502–521.
3. Vandeburgh H, Shansky J, Benesch-Lee F, Barbata V, Reid J, Thorrez L, Valentini R, Crawford G. Drug-screening platform based on the contractility of tissue-engineered muscle. *Muscle Nerve* 2008; 37:438–447.
4. Ko IK, Lee B, Lee SJ, Andersson K, Atala A, Yoo JJ. The effect of *in vitro* formation of acetylcholine receptor (AChR) clusters in engineered muscle fibers on subsequent innervation of constructs *in vivo*. *Biomaterials* 2013; 34:3246–3255.
5. Juhas M, Engelmayer GC, Fontanella AN, Palmer GM, Bursac N. Biomimetic engineered muscle with capacity for vascular integration and functional maturation *in vivo*. *Proc Natl Acad Sci USA* 2014;111:5508–5513.
6. Fuoco C, Rizzi R, Biondo A, Longa E, Mascaro A, Shapira-Schweitzer K, Kossovov O, Benedetti S, Salvatori ML, Santoleri S, Testa S, Bernardini S, Bottinelli R, Bearzi C, Cannata SM, Seliktar

- D, Cossu G, Gargioli C. In vivo generation of a mature and functional artificial skeletal muscle. *EMBO Mol Med* 2015; 7:411–422.
7. Hill E, Boontheekul T, Mooney DJ. Designing scaffolds to enhance transplanted myoblast survival and migration. *Tissue Eng* 2006; 12:1295–1304.
  8. Wang L, Cao L, Shansky J, Wang Z, Mooney D, Vandenburgh H. Minimally invasive approach to the repair of injured skeletal muscle with a shape-memory scaffold. *Mol Ther* 2014;22:1441–1449.
  9. Sicari BM, Rubin JP, Dearth CL, Wolf MT, Ambrosio F, Boninger M, Turner NJ, Weber DJ, Simpson TW, Wyse A, Brown EHP, Dziki JL, Fisher LE, Brown S, Badylak SF. An acellular biologic scaffold promotes skeletal muscle formation in mice and humans with volumetric muscle loss. *Sci Transl Med* 2014;6: 234ra58.
  10. Borselli C, Storrle H, Benesch-Lee F, Shvartsman D, Cezar C, Lichtman JW, Vandenburgh HH, Mooney DJ. Functional muscle regeneration with combined delivery of angiogenesis and myogenesis factors. *Proc Natl Acad Sci USA* 2010;107:3287–3292.
  11. San Emeterio CL, Olingy CE, Chu Y, Botchwey EA. Selective recruitment of non-classical monocytes promotes skeletal muscle repair. *Biomaterials* 2017;117:32–43.
  12. Sung JH, Shuler ML. Microtechnology for mimicking in vivo tissue environment. *Ann Biomed Eng* 2012;40:1289–1300.
  13. Rossi CA, Pozzobon M, De Coppi P. Advances in musculoskeletal tissue engineering: Moving towards therapy. *Organogenesis* 2010;6:167–172.
  14. Huang NF, Patel S, Thakar RG, Wu J, Hsiao BS, Chu B, Lee RJ, Li S. Myotube assembly on nanofibrous and micropatterned polymers. *Nano Lett* 2006;6:537–542.
  15. Yamamoto DL, Csikasz RI, Li Yu, Sharma G, Hjort K, Karlsson R, Bengtsson T. Myotube formation on micro-patterned glass: Intracellular organization and protein distribution in C2C12 skeletal muscle cells. *J Histochem Cytochem* 2008;56:881–892.
  16. Sun Y, Duffy R, Lee A, Feinberg AW. Optimizing the structure and contractility of engineered skeletal muscle thin films. *Acta Biomater* 2013;9:7885–7894.
  17. Aubin H, Nichol JW, Hutson CB, Bae H, Sieminski AL, Crokek DM, Akhyari P, Khademhosseini A. Directed 3D cell alignment and elongation in microengineered hydrogels. *Biomaterials* 2010;31:6941–6951.
  18. Zatti S, Zoso A, Serena E, Luni C, Cimetta E, Elvassore N. Micro-patterning topology on soft substrates affects myoblast proliferation and differentiation. *Langmuir* 2012;28:2718–2726.
  19. Shah R, Knowles JC, Hunt NP, Lewis MP. Development of a novel smart scaffold for human skeletal muscle regeneration. *J Tissue Eng Regen Med* 2013;10:162–171.
  20. Player DJ, Martin NRW, Passey SL, Sharples AP, Mudera V, Lewis MP. Acute mechanical overload increases IGF-I and MMP-9 mRNA in 3D tissue-engineered skeletal muscle. *Biotechnol Lett* 2014;36:1113–1124.
  21. Ito A, Yamamoto Y, Sato M, Ikeda K, Yamamoto M, Fujita H, Nagamori E, Kawabe Y, Kamiyama M. Induction of functional tissue-engineered skeletal muscle constructs by defined electrical stimulation. *Sci Rep* 2014;4:4781.
  22. Heher P, Maleiner B, Prüller J, Teuschl AH, Kollmitzer J, Monforte X, Wolbank S, Redl H, Rünzler D, Fuchs C. A novel bioreactor for the generation of highly aligned 3D skeletal muscle-like constructs through orientation of fibrin via application of static strain. *Acta Biomater* 2015;24:251–265.
  23. Tseng TH, Chu CY, Huang JM, Shiow SJ, Wang CJ. Crocetin protects against oxidative damage in rat primary hepatocytes. *Cancer Lett* 1995;97:61–67.
  24. Sung H. In vitro surface characterization of a biological patch fixed with a naturally occurring crosslinking agent. *Biomaterials* 2000;21:1353–1362.
  25. Koo HJ, Lim KH, Jung HJ, Park EH. Anti-inflammatory evaluation of gardenia extract, geniposide and genipin. *J Ethnopharmacol* 2006;103:496–500.
  26. Bigi A, Cojazzi G, Panzavolta S, Roveri N, Rubini K. Stabilization of gelatin films by crosslinking with genipin. *Biomaterials* 2002; 23:4827–4832.
  27. Montemurro F, De Maria C, Orsi G, Ghezzi L, Tinè MR, Vozzi G. Genipin diffusion and reaction into a gelatin matrix for tissue engineering applications. *J Biomed Mater Res B Appl Biomater* 2017;105:473–480.
  28. Liang H, Chang W, Lin K, Sung H. Genipin-crosslinked gelatin microspheres as a drug carrier for intramuscular administration: In vitro and in vivo studies. *J Biomed Mater Res A* 2003;65:271–282.
  29. Solorio L, Zwolinski C, Lund AW, Farrell MJ, Stegemann JP. Gelatin microspheres crosslinked with genipin for local delivery of growth factors. *J Tissue Eng Regen Med* 2010;4:514–523.
  30. Chang WH, Chang Y, Lai PH, Sung HW. A genipin-crosslinked gelatin membrane as wound-dressing material: In vitro and in vivo studies. *J Biomater Sci Polym Ed* 2003;14:481–495.
  31. Focaroli S, Teti G, Salvatore V, Durante S, Belmonte MM, Giardino R, Mazzotti A, Bigi A, Falconi M. Chondrogenic differentiation of human adipose mesenchymal stem cells: Influence of a biomimetic gelatin genipin crosslinked porous scaffold. *Microsc Res Tech* 2014;77:928–934.
  32. Chen YS, Chang JY, Cheng CY, Tsai FJ, Yao CH, Liu BS. An in vivo evaluation of a biodegradable genipin-cross-linked gelatin peripheral nerve guide conduit material. *Biomaterials* 2005;26: 3911–3918.
  33. Chang J-Y, Ho T-Y, Lee H-C, Lai Y-L, Lu M-C, Yao C-H, Chen Y-S. Highly permeable genipin-cross-linked gelatin conduits enhance peripheral nerve regeneration. *Artif Organs* 2009;33:1075–1085.
  34. Lien SM, Li WT, Huang TJ. Genipin-crosslinked gelatin scaffolds for articular cartilage tissue engineering with a novel crosslinking method. *Mater Sci Eng C* 2008;28:36–43.
  35. Vozzi G, Corallo C, Carta S, Fortina M, Gattazzo F, Galletti M, Giordano N. Collagen-gelatin-genipin-hydroxyapatite composite scaffolds colonized by human primary osteoblasts are suitable for bone tissue engineering applications: In vitro evidences. *J Biomed Mater Res A* 2014;102:1415–1421.
  36. Sharifi E, Azami M, Kajbafzadeh A-M, Moztafzadeh F, Faridi-Majidi R, Shamousi A, Karimi R, Ai J. Preparation of a biomimetic composite scaffold from gelatin/collagen and bioactive glass fibers for bone tissue engineering. *Mater Sci Eng C Mater Biol Appl* 2016;59:533–541.
  37. Carrabba M, De Maria C, Oikawa A, Reni C, Rodriguez-Arabaolazal, Spencer H, Slater S, Avolio E, Dang Z, Spinetti G, Madeddu P, Vozzi G. Design, fabrication and perivascular implantation of bioactive scaffolds engineered with human adventitial progenitor cells for stimulation of arteriogenesis in peripheral ischemia. *Biofabrication* 2016;8:15020.
  38. Boldrin L, Elvassore N, Malerba A, Flaibani M, Cimetta E, Piccoli M, Baroni MD, Gazzola MV, Messina C, Gamba P, Vitiello L, de Coppi P. Satellite cells delivered by micro-patterned scaffolds: A new strategy for cell transplantation in muscle diseases. *Tissue Eng* 2007;13:253–262.
  39. Rossi CA, Flaibani M, Blaauw B, Pozzobon M, Figallo E, Reggiani C, Vitiello L, Elvassore N, De Coppi P. In vivo tissue engineering of functional skeletal muscle by freshly isolated satellite cells embedded in a photopolymerizable hydrogel. *FASEB J* 2011;25: 2296–2304.
  40. Gattazzo F, Molon S, Morbidoni V, Braghetta P, Blaauw B, Urciuolo A, Bonaldo Paolo. Cyclosporin A promotes in vivo myogenic response in collagen VI-deficient myopathic mice. *Front Aging Neurosci* 2014;6:244.
  41. Liu BS, Yao CH, Chen YS, Hsu SH. In vitro evaluation of degradation and cytotoxicity of a novel composite as a bone substitute. *J Biomed Mater Res A* 2003;67:1163–1169.
  42. Engler AJ, Griffin MA, Sen S, Bönnemann CG, Sweeney HL, Discher DE. Myotubes differentiate optimally on substrates with tissue-like stiffness: Pathological implications for soft or stiff microenvironments. *J Cell Biol* 2004;166:877–887.
  43. Gilbert PM, Havenstrite KL, Magnusson KEG, Sacco A, Leonardi NA, Kraft P, Nguyen NK, Thrun S, Lutolf MP, Blau HM. Substrate elasticity regulates skeletal muscle stem cell self-renewal in culture. *Science* 2010;329:1078–1081.
  44. Charest JL, Garcia AJ, King WP. Myoblast alignment and differentiation on cell culture substrates with microscale topography and model chemistries. *Biomaterials* 2007;28:2202–2210.
  45. Bajaj P, Reddy B, Millet L, Wei C, Zorlutuna P, Bao G, Bashir R. Patterning the differentiation of C2C12 skeletal myoblasts. *Integr Biol (Camb)* 2011;3:897–909.
  46. Shen CC, Yang YC, Liu BS. Peripheral nerve repair of transplanted undifferentiated adipose tissue-derived stem cells in a

- biodegradable reinforced nerve conduit. *J Biomed Mater Res A* 2012;100:48–63.
47. Engler AJ, Sen S, Sweeney HL, Discher DE. Matrix elasticity directs stem cell lineage specification. *Cell* 2006;126:677–689.
  48. Boonthekul T, Hill EE, Kong H-J, Mooney DJ. Regulating myoblast phenotype through controlled gel stiffness and degradation. *Tissue Eng* 2007;13:1431–1442.
  49. Jun I, Jeong S, Shin H. The stimulation of myoblast differentiation by electrically conductive sub-micron fibers. *Biomaterials* 2009;30:2038–2047.
  50. Shimizu K, Fujita H, Nagamori E. Alignment of skeletal muscle myoblasts and myotubes using linear micropatterned surfaces ground with abrasives. *Biotechnol Bioeng* 2009;103:631–638.
  51. Huang NF, Lee RJ, Li S. Engineering of aligned skeletal muscle by micropatterning. *Am J Transl Res* 2010;2:43–55.
  52. Serena E, Zatti S, Reghelini E, Pasut A, Cimetta E, Elvassore N. Soft substrates drive optimal differentiation of human healthy and dystrophic myotubes. *Integr Biol (Camb)* 2010;2:193–201.
  53. Ku SH, Lee SH, Park CB. Synergic effects of nanofiber alignment and electroactivity on myoblast differentiation. *Biomaterials* 2012;33:6098–6104.
  54. Hosseini V, Ahadian S, Ostrovidov S, Camci-Unal G, Chen S, Kaji H, Ramalingam M, Khademhosseini A. Engineered contractile skeletal muscle tissue on a microgrooved methacrylated gelatin substrate. *Tissue Eng A* 2012;18:2453–2465.
  55. Monge C, Ren K, Berton K, Guillot R, Peyrade D, Picart C. Engineering muscle tissues on microstructured polyelectrolyte multilayer films. *Tissue Eng A* 2012;18:1664–1676.
  56. Sengupta D, Gilbert PM, Johnson KJ, Blau HM, Heilshorn SC. Protein-engineered biomaterials to generate human skeletal muscle mimics. *Adv Healthc Mater* 2012;1:785–789.
  57. Shimizu K, Fujita H, Nagamori E. Micropatterning of single myotubes on a thermoresponsive culture surface using elastic stencil membranes for single-cell analysis. *J Biosci Bioeng* 2010;109:174–178.
  58. Chen MC, Sun YC, Chen YH. Electrically conductive nanofibers with highly oriented structures and their potential application in skeletal muscle tissue engineering. *Acta Biomater* 2013;9:5562–5572.
  59. Bettadapur A, Suh GC, Geisse NA, Wang ER, Hua C, Huber HA, Viscio AA, Kim JY, Strickland JB, McCain ML. Prolonged culture of aligned skeletal myotubes on micromolded gelatin hydrogels. *Sci Rep* 2016;6:28855.
  60. Hwang YJ, Larsen J, Krasieva TB, Lyubovitsky JG. Effect of genipin crosslinking on the optical spectral properties and structures of collagen hydrogels. *ACS Appl Mater Interfaces* 2011;3:2579–2584.
  61. Perniconi B, Costa A, Aulino P, Teodori L, Adamo S, Coletti D. The pro-myogenic environment provided by whole organ scale acellular scaffolds from skeletal muscle. *Biomaterials* 2011;32:7870–7882.
  62. Hurd SA, Bhatti NM, Walker AM, Kasukonis BM, Wolchok JC. Development of a biological scaffold engineered using the extracellular matrix secreted by skeletal muscle cells. *Biomaterials* 2015;49:9–17.
  63. Wang L, Shansky J, Borselli C, Mooney D, Vandenburgh H. Design and fabrication of a biodegradable, covalently crosslinked shape-memory alginate scaffold for cell and growth factor delivery. *Tissue Eng A* 2012;18:2000–2007.
  64. Anderson JM, Rodriguez A, Chang DT. Foreign body reaction to biomaterials. *Semin Immunol* 2008;20:86–100.
  65. Tidball JG, Villalta SA. Regulatory interactions between muscle and the immune system during muscle regeneration. *Am J Physiol Regul Integr Comp Physiol* 2010;298:R1173–1187.
  66. Mantovani A, Biswas SK, Galdiero MR, Sica A, Locati M. Macrophage plasticity and polarization in tissue repair and remodelling. *J Pathol* 2013;229:176–185.
  67. Fishman JM, Lowdell MW, Urbani L, Ansari T, Burns AJ, Turmaine M, North J, Sibbons P, Seifalian AM, Wood KJ, Birchall MA, De Coppi P. Immunomodulatory effect of a decellularized skeletal muscle scaffold in a discordant xenotransplantation model. *Proc Natl Acad Sci USA* 2013;110:14360–14365.
  68. Ma J, Holden K, Zhu J, Pan H, Li Y. The application of three-dimensional collagen scaffolds seeded with myoblasts to repair skeletal muscle defects. *J Biomed Biotechnol* 2011;2011:1–9.
  69. Mase VJ, Hsu JR, Wolf SE, Wenke JC, Baer DG, Owens J, Badylak SF, Walters TJ. Clinical application of an acellular biologic scaffold for surgical repair of a large, traumatic quadriceps femoris muscle defect. *Orthopedics* 2010;33:511.
  70. JA DeQuach, JE Lin, C Cam, D Hu, MA Salvatore, F Sheikh, KL Christman. Injectable skeletal muscle matrix hydrogel promotes neovascularization and muscle cell infiltration in a hindlimb ischemia model. *Eur Cells Mater* 2012;23:400–412.
  71. Yang HS, Ieronimakis N, Tsui JH, Kim HN, Suh K-Y, Reyes M, Kim D-H. Nanopatterned muscle cell patches for enhanced myogenesis and dystrophin expression in a mouse model of muscular dystrophy. *Biomaterials* 2014;35:1478–1486.
  72. Vasconcelos DP, Costa M, Amaral IF, Barbosa MA, Águas AP, Barbosa JN. Development of an immunomodulatory biomaterial: Using resolvin D1 to modulate inflammation. *Biomaterials* 2015;53:566–573.
  73. Alvarez MM, Liu JC, Trujillo-de Santiago G, Cha B-H, Vishwakarma A, Ghaemmaghami AM, Khademhosseini A. Delivery strategies to control inflammatory response: Modulating M1-M2 polarization in tissue engineering applications. *J Control Release* 2016;240:349–363.